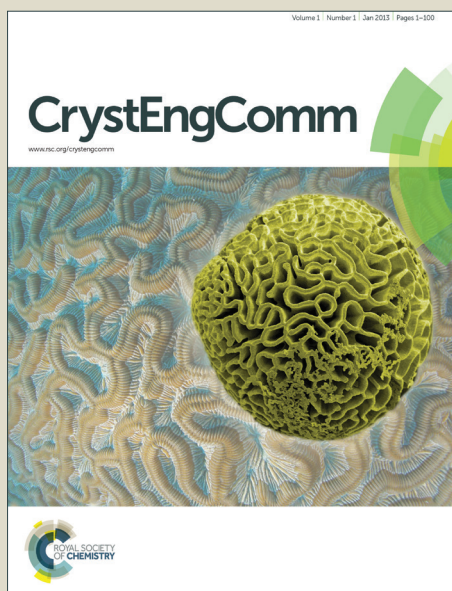


CrystEngComm

Accepted Manuscript



This is an *Accepted Manuscript*, which has been through the Royal Society of Chemistry peer review process and has been accepted for publication.

Accepted Manuscripts are published online shortly after acceptance, before technical editing, formatting and proof reading. Using this free service, authors can make their results available to the community, in citable form, before we publish the edited article. We will replace this *Accepted Manuscript* with the edited and formatted *Advance Article* as soon as it is available.

You can find more information about *Accepted Manuscripts* in the [Information for Authors](#).

Please note that technical editing may introduce minor changes to the text and/or graphics, which may alter content. The journal's standard [Terms & Conditions](#) and the [Ethical guidelines](#) still apply. In no event shall the Royal Society of Chemistry be held responsible for any errors or omissions in this *Accepted Manuscript* or any consequences arising from the use of any information it contains.

ARTICLE

Quantum mechanical predictions to elucidate the anisotropic elastic properties of zeolitic imidazolate frameworks: ZIF-4 vs. ZIF-zni

Cite this: DOI: 10.1039/x0xx00000x

Jin-Chong Tan,^{*a} Bartolomeo Civalleri,^{‡b} Alessandro Erba^b and Elisa Albanese^bReceived 00th January 2012,
Accepted 00th January 2012

DOI: 10.1039/x0xx00000x

www.rsc.org/

We use *ab initio* density functional theory (DFT) to elucidate the mechanical properties of two topologically distinct zeolitic imidazolate framework (ZIF) materials: ZIF-4 and ZIF-zni, both of which have the same chemical composition $\text{Zn}(\text{Im})_2$ [$\text{Im} = \text{C}_3\text{H}_3\text{N}_2^-$] and constructed from an identical $\text{Zn}-\text{Im}-\text{Zn}$ basic building block. The CRYSTAL code was used to compute the single-crystal elastic constants C_{ij} 's of the (orthorhombic) ZIF-4 and (tetragonal) ZIF-zni structures, at the PBE level of theory. Through tensorial analysis of the C_{ij} 's, we reveal the three-dimensional representation surfaces of the Young's modulus, shear modulus, Poisson's ratio and linear compressibility, which enable us to describe the detailed elasticity behaviour and to pinpoint basic crystal structure-property correlations. Notably, we discover that ZIF-4 can potentially exhibit negative Poisson's ratio, thereby representing the first example of an 'auxetic-ZIF' to be identified to date. Furthermore, we show that our DFT predictions are consistent with recently reported experimental measurements of the Young's and bulk moduli of such complex ZIF structures.

1. Introduction

Zeolitic imidazolate frameworks (ZIFs)^{1,2} belong to a rapidly expanding class of nanoporous hybrid materials, known as metal-organic frameworks (MOFs). Noted for their three-dimensional framework topologies akin to inorganic zeolites, ZIFs exhibit promising physico-chemical characteristics that are central to many emergent technologies.^{3,4} Recently we have witnessed a growing body of work associated with the mechanical properties of MOFs, which has been instigated by both fundamental and practical motivations.⁵ Below we outline a few representative exemplars to illustrate the upward trend in this growing topic area.

First, information on the mechanical properties of MOFs, encompassing elasticity and hardness,^{6,7} fracture toughness⁸ and cohesive strength of interfaces⁹ are key towards the optimisation and fabrication of novel electrodes, thin-film sensors¹⁰ and microelectronic devices.¹¹ Second, first-principles calculations have enabled predictions of single-crystal elastic constants,^{12,13} their anisotropy,¹⁴ and to gain insights into plastic deformation behaviour beyond the elastic limit.¹⁵ Moreover, theoretical studies could offer clues into probable mechanisms responsible for structural destabilisation.¹⁶ Third, the application of high-pressure experiments under hydrostatic

conditions has enabled the determination of bulk modulus,¹⁷⁻¹⁹ alongside the detection of negative linear compressibility in MOFs.²⁰ Fourth, the discovery of facile collapse of ZIFs *via* mechanical- and temperature-induced amorphisation^{21,22} emphasises the role of thermo-mechanical stability for leveraging the amorphisation process to afford novel applications involving, for instance, irreversible trapping of radioactive isotopes and harmful chemical substances.²³ Ultimately with improved knowledge of MOF elasticity and mechanical characteristics, commercial materials processing routes could be devised to enable high-throughput shaping of MOF powders into pellets and extrudates, without sacrificing porosity (due to collapse) and chemical functionalities.²⁴

In this work, we have employed density-functional theory (DFT) to investigate the detailed elastic behaviour of two relatively well-known ZIF-type materials, termed ZIF-4 and ZIF-zni.^{1,4} More specifically, both frameworks feature an identical chemical composition [$\text{Zn}(\text{C}_3\text{H}_3\text{N}_2)_2$], whereby the inorganic and organic building units comprise the divalent Zn^{2+} metal cation and an unsubstituted imidazolate ligand [$(\text{C}_3\text{H}_3\text{N}_2)^-$], respectively. However, as depicted in Fig. 1, their crystallographic structures, network topologies and void characteristics are substantially different.

Table 1 Single-crystal elastic stiffness constants (C_{ij} 's) of ZIF-4 and ZIF-zni determined from density functional theory.

C_{ij} (GPa)	NIEC $^\diamond$	C_{11}	C_{22}	C_{33}	C_{44}	C_{55}	C_{66}	C_{12}	C_{13}	C_{23}
ZIF-4	9	4.266	3.492	5.015	1.029	1.927	2.453	1.221	1.916	1.526
ZIF-zni	6	19.010	$= C_{11}$	23.384	1.557	$= C_{44}$	1.759	13.257	13.377	$= C_{13}$

$^\diamond$ Number of independent elastic constants.

Interestingly it was recently discovered that, porous ZIF-4 (solvent accessible volume, SAV \sim 29%) undergoes a crystalline-amorphous transformation when heated to 300 °C,²² which upon further heating (400 °C) recrystallises into the ZIF-zni phase (SAV \sim 12%).²⁵ The latter represents the thermodynamically most stable as well as the *densest* crystalline ZIF phase. We note that the *narrow* pores in ZIF-4 can be accessed (BET surface area \sim 300 m² g⁻¹) through a *gate-opening* mechanism activated at low pressure (\sim 35 kPa).²⁶ While measurements of the Young's modulus (E) and bulk modulus (K) of ZIF-4 and ZIF-zni have previously been conducted,^{7,22,25} the fundamental elastic constants (C_{ij} 's) of both phases have yet to be established. Basic knowledge of C_{ij} 's will enable one to elucidate the complete set of elastic properties and to pinpoint any anisotropic elastic behaviour, beyond the two elastic moduli reported so far. Importantly, the availability of experimental E and K values also means that validation of the accuracy and reliability of our theoretical predictions can be performed.

analogous to that of the Si-O-Si characteristic angle in inorganic zeolites (aluminosilicates). (b) Orthorhombic unit cell of ZIF-4 and (c) tetragonal unit cell of ZIF-zni, showing their framework architecture and topology. ZnN₄ coordination tetrahedra (in pink) represent the inorganic building units. (d),(e) Yellow surfaces denote the solvent accessible volume (SAV) of the pores, determined using a probe radius of 1.2 Å with a grid spacing of 0.5 Å (via the 'Voids' algorithm implemented in Mercury CSD).²⁷ Color scheme used: zinc: purple; carbon: grey; nitrogen: blue; hydrogen: white.

2. Computational Methodology

We performed density functional theory (DFT) calculations using the *ab initio* CRYSTAL09 periodic code,²⁸ based on the atom-centred Gaussian-type basis set. The single-crystal elastic stiffness constants, C_{ij} 's, were computed with the PBE exchange-correlation functional²⁹ and using an all-electron basis set of double-zeta quality. More precisely, for carbon, nitrogen and hydrogen atoms the 6-31G(d,p) basis set was adopted, while the 8s-64111sp-31d-1f was used for Zn; this basis set has been successfully implemented in a previous work on MOF-5.³⁰ An unconstrained geometry optimisation of the lattice parameters and atomic positions for both ZIFs was carried out by tightening the default convergence criteria by an order of magnitude (see details in ESI†). On the optimized structures, the independent elastic constants were computed by using an automatic procedure developed by Perger *et al.*³¹ The numerical first-derivative of the analytic cell gradients, which corresponds to the elastic stiffness coefficients C_{ij} 's was computed by using a three-point formula and subjecting the unit cell to a 'small' adimensional deformation, corresponding to an externally applied (normal or shear) strain of up to $\pm 1\%$.

3. Results and Discussion

Table 1 summarises all the computed single-crystal elastic coefficients, C_{ij} 's. Orthorhombic ZIF-4 has nine independent elastic constants, which are reduced to six independent elements for (tetragonal) ZIF-zni, by virtue of the higher symmetry of the latter (Fig. 1).

On the main diagonal of the elastic tensor (ESI†), the coefficients C_{11} , C_{22} and C_{33} respectively indicate the stiffnesses along the three orthonormal a -, b -, and c -principal crystal axes under uniaxial strains; the shear coefficients C_{44} , C_{55} and C_{66} signify the stiffness against angular distortions when subjected to shear strains. Finally, coefficients containing mixed subscripts, *i.e.* C_{12} , C_{13} and C_{23} , correspond to tensile-tensile couplings between any two orthonormal axes. Here we note there is neither tensile-shear (*e.g.* $C_{14} = C_{25} = C_{36} = 0$), nor

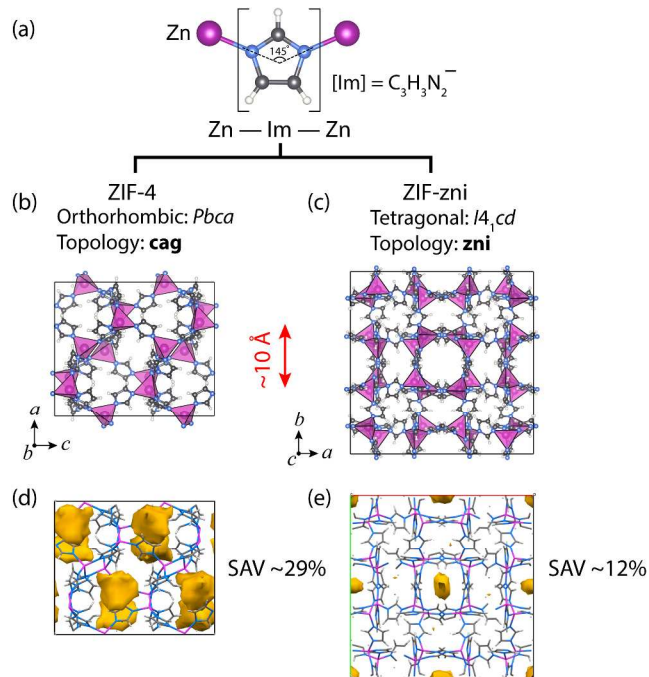


Fig. 1 Crystal structures of ZIF-4 and ZIF-zni, exhibiting the same chemical composition Zn(C₃H₃N₂)₂. (a) Zn—Im—Zn basic building unit, in which Zn²⁺ are tetrahedral metal centres coordinated by nitrogen atoms at the 1,3-positions of the imidazolate (Im) bridging ligand. The subtended angle at the Zn—Im—Zn centre is $\sim 145^\circ$, which is

shear-shear couplings ($C_{45} = C_{46} = C_{56} = 0$) for crystals exhibiting orthorhombic and tetragonal symmetry (since lattice angles $\alpha = \beta = \gamma = 90^\circ$). In the subsequent sections, we shall describe how tensorial analysis³² of the elastic constants C_{ij} 's (via ELAM code³³) can be used to describe the complete elastic behaviour of ZIF-4 and ZIF-zni. A summary of the maximal and minimal magnitudes together with the extent of elastic anisotropy are summarised in Table 2.

Table 2 Single-crystal elastic properties of ZIF-4 and ZIF-zni calculated based on the independent elastic constants C_{ij} 's of Table 1.

Elastic properties		ZIF-4	ZIF-zni
Young's modulus, E (GPa)	E_{\max}	4.54	12.29
	E_{\min}	2.76	4.69
	$A_E = E_{\max}/E_{\min}$	1.64	2.62
Shear modulus, G (GPa)	G_{\max}	2.45	3.77
	G_{\min}	1.03	1.56
	$A_G = G_{\max}/G_{\min}$	1.87	2.42
Linear compressibility, β (TPa ⁻¹)	β_x	138.65	25.23
	β_y	200.57	25.23
	β_z	85.40	13.90
Poisson's ratio, ν (-)	ν_{\max}	0.47	0.67
	ν_{\min}	-0.11	0.20
Ledbetter anisotropy [†]	A^*	2.38	2.47

[†] A^* is defined as the ratio of the maximum and minimum shear sound wave velocities.³⁴

3.1 Young's Modulus (E)

We start by examining the Young's modulus (E), which is defined as the ratio of normal stress (σ) to normal strain (ϵ) under an uniaxial loading condition (1-D stress state). The Young's modulus thereby captures the fully reversible stiffness response as in a linear elastic Hookean spring. Though in a single crystal, the magnitudes of the Young's moduli are typically directionally dependent, *i.e.* anisotropic.

The 3-D representation surfaces shown in Fig. 2(a,b) clearly indicate that the Young's moduli of both ZIF crystals are directionally dependent. We found that ZIF-zni is considerably more anisotropic than ZIF-4, with the corresponding A_E ratios (E_{\max}/E_{\min} in Table 2) of ~ 2.6 and ~ 1.6 , respectively. Evidently both structures are relatively more anisotropic than the prototypical ZIF-8 with a sodalite topology, whose A_E is 1.35;¹³ this comparison confirms that ZIF-zni is approximately twice more anisotropic than the cubic ZIF-8, with regards to E . Fig. 2b supports this finding where there are six distinct protuberances along the principal axes of ZIF-zni, all of which directly linked to the greater structural stiffness conferred by the continuous Zn—Im—Zn linkages akin to 'chains' (Fig. 1a) running along the principal axes.

For ZIF-zni, we established the highest E value (~ 12 GPa) along the $\langle 001 \rangle$ zone axes, in accordance with the continuous

Zn—Im—Zn connectivity prevalent on that precise orientation, as illustrated in Fig. 2f. Likewise, we witnessed the same structure-property correlation in the case of ZIF-4 (Fig. 2c,e) with maximum E values (~ 4.5 GPa) identified in the proximity of the $\langle 101 \rangle$ axes, albeit the magnitude of which is markedly lower ($\sim 60\%$) due to the greater porosity in ZIF-4 (see comparison of SAV% in Fig. 1). It is, of course, also of great relevance to pinpoint the mechanically more compliant ('soft') directions on which lie the minimum Young's moduli (Table 2 and Fig. 2c,d). Herein, we established that any crystallographic orientations deviating from the primary 'backbone' axis of the Zn—Im—Zn building units (Fig. 2e,f) are bound to possess a greater compliance (hence lower stiffness).

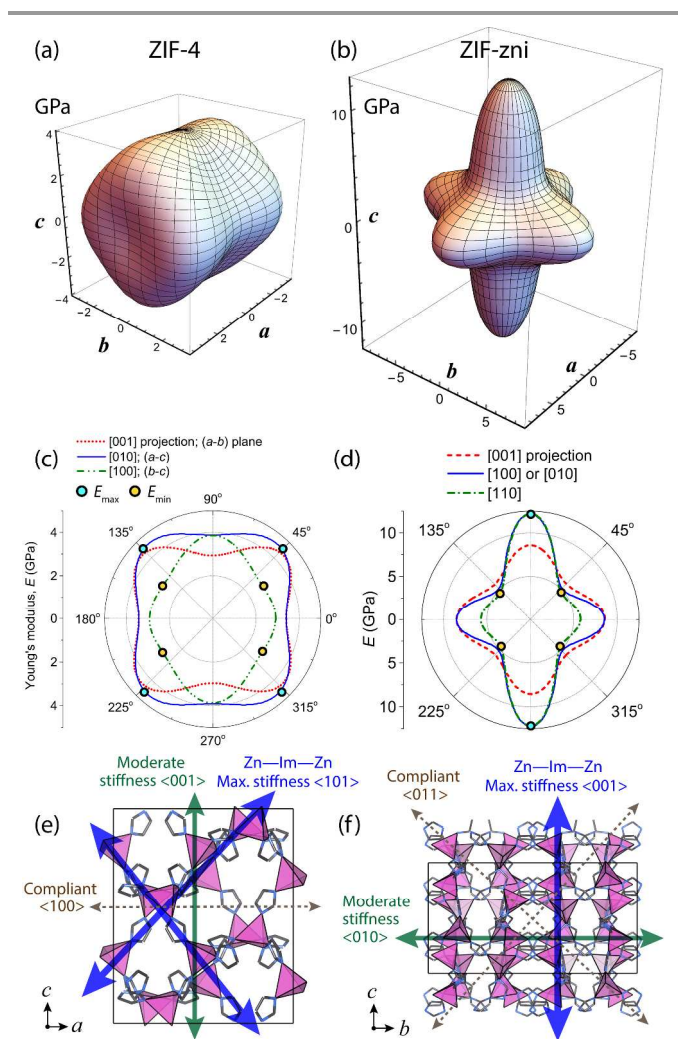


Fig. 2 Young's modulus (E) representation surface. (a) ZIF-4 with E_{\max} lying in the proximity of the $\langle 101 \rangle$ zone axes, whereas E_{\min} found along the $\langle 032 \rangle$ axes. (b) ZIF-zni, featuring E_{\max} along the $\langle 001 \rangle$ while E_{\min} is almost coincident with the $\langle 111 \rangle$ orientations. (c),(d) Corresponding polar plots obtained *via* projections through the origin onto the three orthonormal planes, showing the positions of maximum and minimum moduli. Because of tetragonal symmetry of ZIF-zni, projections down the $[100]$ and $[010]$ axes are identical. (e),(f) Molecular structure-stiffness property correlations in ZIF-4 and ZIF-zni respectively, where the thickness of the lines and the size of the arrow

heads represent the magnitude of the stiffness (E) in that particular orientation.

It is most encouraging to see that the present theoretical predictions are consistent with experimentally determined Young's moduli from single-crystal nanoindentation. For example, nanoindentation measurements of ZIF-4 reported $E\{111\} \approx E\{100\} \sim 4.6$ GPa, and that of ZIF-zni reported $E\{001\} \sim 9$ GPa and $E\{100\} \sim 8$ GPa.⁷ Here we note that the corresponding predicted moduli are: ZIF-4 (3.4–3.9 GPa) and ZIF-zni (12 and 8.6 GPa), respectively. Whilst the agreement in terms of magnitude and anisotropy is noteworthy, here we would like to highlight the two major sources of errors. First, from the experimental perspective, discrepancy arises from the fact that the standard nanoindentation analysis (Pharr and Oliver method)³⁵ treats the material as an isotropic continuum, additionally the stress state under the indenter tip is not strictly uniaxial during loading,^{8,36} which is compounded by possible crystallographic misalignments during mounting of single crystals. Second, from the theoretical point of view, DFT computations by default assume a defect-free ('perfect') crystalline structure with calculated C_{ij} 's corresponding to 0 K, furthermore the numerical accuracy of DFT predictions could be sensitive to, for instance, the subtle choices of different Hamiltonians.^{13,37}

3.2 Shear Modulus (G)

The shear or rigidity modulus, G , represents the resistance against shape change or angular geometrical distortions (*i.e.* shear strain γ) under the influence of an opposing pair of shear stresses, τ , acting parallel to the material surface. On this basis, a framework possessing a higher structural 'rigidity' towards shear strain would exhibit a greater magnitude of G . In line with the Young's modulus characteristics discussed in §3.1, the shear modulus of ZIF-zni is relatively more anisotropic than that of ZIF-4; their G_{\max}/G_{\min} ratios (A_G) are 2.42 and 1.87 respectively, which are better visualised *via* 3-D maximal and minimal shear representation surfaces in Fig. 3.

Compared with the prototypical ZIF-8 ($G \sim 1$ GPa),¹³ clearly both materials exhibit an increased resistance towards shear deformation (Table 2), with a factor of at least 2–3 times higher. It is striking to discover that, the minimum value of shear modulus (G_{\min}) for ZIF-zni that represents the 'densest' ZIF structure, to be lying just at ~ 1.6 GPa. Hence we speculate that this value may represent the G_{\min} upper-bound of all ZIF-type materials. This finding further substantiates the recent proposal¹³ asserting that ZIFs display great propensity to stress-induced amorphisation (*e.g.* ball-milling and pressure-induced compaction),²¹ attributable to their relatively small shear moduli compared with inorganic zeolites (G of 20–50 GPa).^{5,13}

The source of such a small shear resistance (G_{\min}) can be understood purely by examining the 4-membered ring (4MR) rectangular configuration (Fig.3f) of ZIF-zni, which is susceptible to shear forces from structural stability standpoint because the four corner-sharing 'nodes' are compliant ZnN_4 tetrahedra, whereas the imidazolate ligands (Im) acting as rigid

bridging linkers.^{13,17} In fact, this molecular connectivity is analogous to a pin-jointed truss mechanism that is intrinsically unstable under shear forces. The same argument applies also to the 4MR of ZIF-4. In light of this, we anticipate that this observation could be a common characteristic of the entire ZIF family⁴ featuring the 4MR structural configuration.

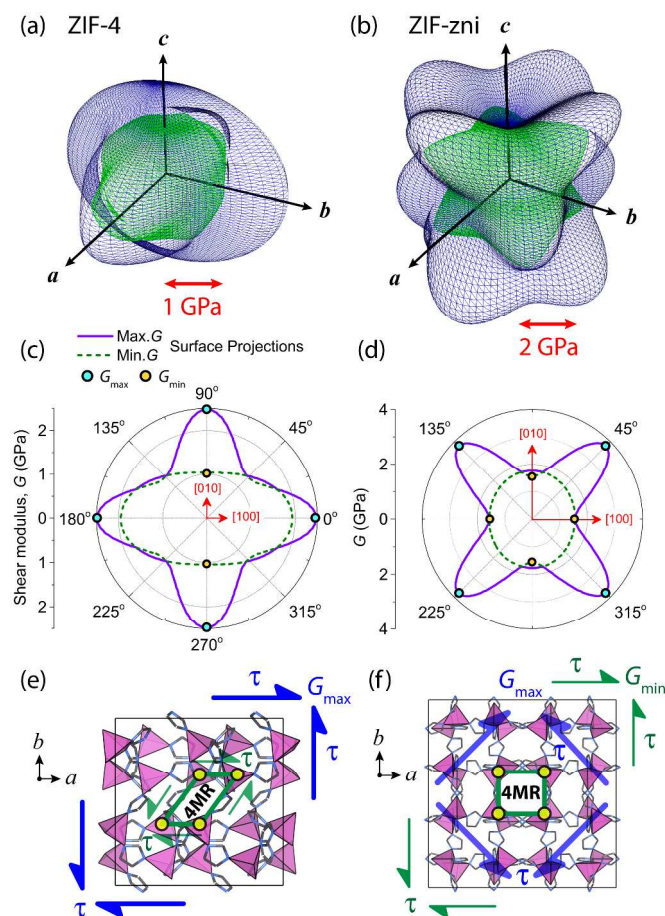


Fig. 3 Shear modulus (G) representation surface of (a) ZIF-4 and (b) ZIF-zni, where blue and green colour coding denotes the maximum and minimum moduli, respectively, at each (θ, ϕ, χ) point in 3-D spherical coordinates. The convention adopted here is in accordance to that proposed by Marmier *et al.*³³ (c),(d) Polar plots are projections through the origin and down the c -axis, showing the positions of maximal and minimal shear moduli. For ZIF-4, G_{\max} is found along the a - and b -axes, whereas G_{\min} identified along the b - and c -axes. For ZIF-zni, G_{\max} is located in the $\langle 110 \rangle$ axes while G_{\min} detected on all three principal axes. (e),(f) Structure-property relationships illustrating the source of the maximal shear moduli, in relation to the position of the 4-membered ring (4MR) which has low rigidity against shear deformation. Shear stresses in blue generate G_{\max} while the opposite pairs in green resulting in G_{\min} . *N.B.* The 4MR in ZIF-4 appears to be oblique since it is not in plane to the a - b projection.

3.3 Poisson's Ratio (ν)

Under uniaxial deformation (tensile or compressive), the ratio of the transverse strain (ϵ_t) to the axial strain (ϵ_a) is termed the Poisson's ratio, *viz.* $\nu = -\epsilon_t/\epsilon_a$; the negative sign designates the contraction (shrinkage) experienced in the transverse direction as the material stretches axially (*i.e.* elongates in the loading axis), and *vice versa*. Table 2 provides a summary of

the maximum and minimum ν values. Compared with ZIF-4, we recognise that ZIF-zni displays a relatively higher $\nu_{\max} \sim 0.7$, which exceeds the upper limit of $\nu = 1/2$ of an incompressible isotropic solid, such as rubber.³⁸

This dimensionless material property ν can be utilised to identify anomalous elastic behaviour, in particular *auxeticity*,^{38,39} where there is an ‘abnormal’ transverse expansion caused by a positive axial strain (and *vice versa*), resulting in effectively a negative Poisson’s ratio (NPR). Tensorial analysis revealed that ZIF-4 is auxetic in certain crystallographic orientations, with $\nu_{\min} = -0.11$, as shown in Fig. 4(a,c). The DFT simulations give further insights into the basis behind auxeticity of ZIF-4. We pinpointed that this abnormal elastic phenomenon occurs when the axial strain (loading direction) is acting along the $\langle 110 \rangle$ axis, yielding a transverse strain of equal sign but directed at the $\langle \bar{1}\bar{1}0 \rangle$ orientation, as illustrated in Fig. 4e. We rationalise that the dominant mechanism responsible for this elastic abnormality involves structural expansion of the initially ‘folded’ 6MR in ZIF-4 (Fig. 4e), in response to a tensile strain directed at the $\langle 110 \rangle$ direction.

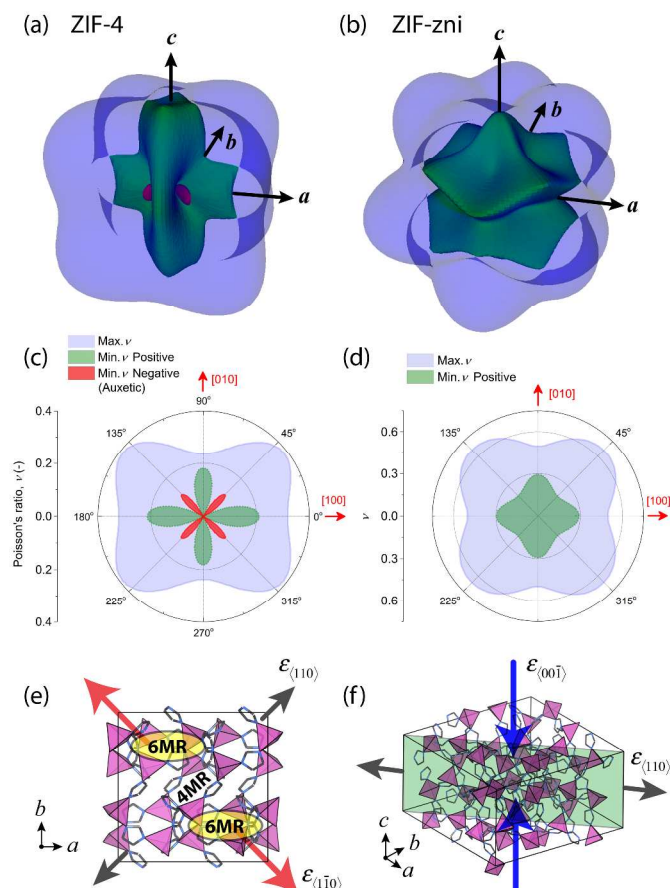


Fig. 4 Poisson’s ratio (ν) representation surface of (a) ZIF-4 and (b) ZIF-zni and their corresponding projections on the a - b plane, as viewed down the $[001]$ axis. The transparent blue surface signifies maximum ν . The minimum ν surface presented in green denotes a positive minimum, while red is used to represent a negative minimum or an auxetic response. The adopted convention follows that proposed in Ref. 33. For ZIF-4, ν_{\max} occurs when loading direction is along the *ca.*

$[11\bar{1}]$ axes accompanied by a lateral contraction in $[111]$; ν_{\min} (auxetic) occurs when loading direction is along $[110]$ producing an ‘unexpected’ lateral expansion along $[1\bar{1}0]$. For ZIF-zni, ν_{\max} is identified when an approximately $[101]$ axial load resulting in a lateral contraction in *ca.* $[10\bar{1}]$; ν_{\min} corresponds to an $[110]$ axial tension yielding a contraction along the $[00\bar{1}]$ direction. Axial and accompanying transverse directions giving rise to the (e) negative ν_{\min} in ZIF-4 and (f) a positive ν_{\min} in ZIF-zni. Grey arrows indicate the directions of loading; red and blue arrows represent expansion and contraction, respectively. Note that symmetry of the original crystal is being reduced upon subjecting to elastic deformation in specific orientations.

The above finding is important because ZIF-4 represents the first example of auxeticity identified within the very broad class of ZIF-type materials, whose open-framework structures to date have been perceived to be ‘not so flexible’ or ‘rigid’,⁴⁰ as such ZIFs are commonly thought to be lacking the propensity to demonstrate (any) anomalous elasticity. Our results highlight that there may be exceptions mainly because some degree of flexibility may arise as a combination of compliant ZnN_4 coordination environment^{13,17} in conjunction with certain topology (*e.g.* **cag** in ZIF-4). In contrast, we note that auxeticity appears to be ubiquitous for extremely flexible MIL-type frameworks (those capable of *breathing* deformation),⁴¹ for which several auxetic examples have recently been predicted from DFT,¹⁴ albeit yet to be experimentally confirmed.

3.4 Linear Compressibility (β) and Bulk Modulus (K)

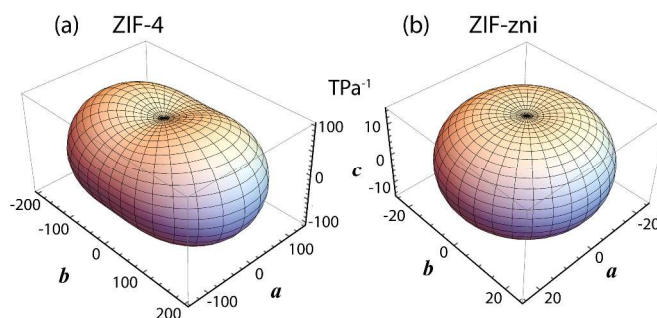


Fig. 5 Linear compressibility (β) representation surface of (a) ZIF-4 and (b) ZIF-zni.

Tensorial analysis of the single crystal C_{ij} ’s (Table 1) has enabled us to determine the anisotropic compressibility (β), as shown in Fig. 5 with corresponding magnitudes along the orthonormal axes summarised in Table 2. It can be seen that ZIF-zni is transversely isotropic (Fig. 5b), *viz.* $\beta_{\langle uv0 \rangle} \sim 25 \text{ TPa}^{-1}$, which is attributable to tetragonal symmetry. More specifically, it exhibits minimum compressibility along the c -axis ($\beta_z \sim 14 \text{ TPa}^{-1}$), on which lie the primary ‘backbone’ of the Zn—Im—Zn continuous chains, thereby providing the additional structural reinforcement to counter compressive forces acting in the $\langle 001 \rangle$ orientation.

Turning to ZIF-4, it can be seen that its linear compressibilities are about an order of magnitude higher; for example, its minimum and maximum linear compressibilities are determined to be ~ 85 and $\sim 200 \text{ TPa}^{-1}$, respectively. Of course, such higher compressibilities are straightforwardly

linked to the larger pore volume present in ZIF-4 (Fig. 1d), which could accommodate volumetric strains. Despite ZIF-4's negative Poisson's ratio (NPR) discussed in §3.3, we established that there is no corresponding 'negative' linear compressibility (NLC) to be detected. This finding is unlike recent DFT predictions¹⁴ that demonstrate NLC and NPR anomalies to go hand-in-hand for 'flexible' MIL-type materials, which is thought to be connected to extreme elastic anisotropy where A_E and A_G typically exceed ~ 100 . Our new results together with literature^{7,13} suggest that such extreme anisotropy might be a rarity for ZIF-type materials.

3.5 Averaged Elastic Properties of Polycrystalline ZIFs

In this section, we shall focus on the predictions of isotropic elastic properties for a texture-free polycrystalline ZIF material. A summary of the results are presented in Table 3. Knowledge of the averaged elastic behaviour is, of course, highly relevant to practical applications of MOFs, many of which will involve preparation of commercial products assuming various forms and sizes, ranging from loose-powder blends to dense compacts, and from polycrystalline coatings to precisely shaped extrusions.^{24,42}

Table 3 Isotropic aggregate elastic properties based on the Voigt-Reuss-Hill (VRH) averages,³² corresponding to a texture-free polycrystalline material. The bulk (K), Young's (E), and shear (G) moduli are in GPa. The Poisson's ratio (ν) is dimensionless.

Property	K_{VRH}	E_{VRH}	G_{VRH}	ν_{VRH}
ZIF-4	2.41	3.82	1.55	0.24
ZIF-zni	15.63	6.37	2.23	0.44

The bulk modulus (K) is an isotropic measure that quantifies the resistance of the structure towards a volumetric strain ($\Delta V/V$), when subjected to a hydrostatic stress state (pressure). Experimental values obtained from high-pressure crystallographic studies are available for validation of current DFT predictions. Our calculations have determined bulk moduli of ZIF-4 and ZIF-zni at $K \sim 2.4$ GPa and ~ 15.6 GPa respectively, implying that the former is almost seven times more compressible than the latter, by virtue of its larger SAV that better affords volumetric strain. The level of agreement against the reported single-crystal high-pressure experiments is impressive, with errors of just $\sim 10\%$: Bennett *et al.*¹⁸ reported bulk modulus of ZIF-4 to be ~ 2.6 GPa, while Spencer *et al.*²⁵ determined bulk modulus of ZIF-zni as ~ 14 GPa. These results are reassuring and highlight the good accuracy obtainable through our computational methodology.

We finally consider the Poisson's ratio of an isotropic aggregate according to the Voigt-Reuss-Hill (VRH) approach. Important to note is that all ν_{VRH} values are indeed positive (Table 3). Though the ZIF-4 single crystal has been predicted to be auxetic (§3.3), its averaged Poisson's ratio corresponding to that of a textureless polycrystal is actually positive ($\nu_{VRH} = 0.24$). That means, in order to exploit the auxetic response of

ZIF-4 assuming the form of an isotropic polycrystalline material, for example, thin-film coatings need to be fabricated in a controlled fashion to realise unidirectional crystal growth strictly in the desirable $\langle 110 \rangle$ axis, on which auxeticity is prominent in ZIF-4. Another challenge lies in the crystal engineering of strongly textured bulk material from ZIF-4 containing the preferred $\langle 110 \rangle$ orientation.

4. Concluding Remarks

In this work, we have employed the theoretical approach by means of *ab initio* density functional theory (DFT) to elucidate the complex elastic behaviour of two topical metal-organic frameworks (MOFs), namely ZIF-4 and ZIF-zni, belonging to the subfamily of zeolitic imidazolate frameworks (ZIFs). While both nanoporous materials have the same chemical composition and constructed from the same Zn—Im—Zn building block, each structure has unique framework architecture and distinct topological features. Our comprehensive results have revealed their anisotropic elastic characteristics, ranging from the Young's modulus to Poisson's ratio, and from linear compressibility to isotropic polycrystalline properties. It is fascinating to be able to establish the underlying structure-property correlations that are key to rationalising the source of directionally-dependent mechanical behaviour. Crucially with the availability of experimental results, specifically using literature E and K values, we were able to convincingly show that our computational results are reliable and accurate (*ca.* 10–20%) in view of the possible deficiencies associated with existing experiments and theory. Notably, we discover that ZIF-4 can exhibit auxeticity (NPR), for which we further pinpointed the specific crystallographic orientations of this anomalous effect together with the potential accompanying molecular mechanism. This is a significant find, as it represents the first example of an 'auxetic-ZIF' to be reported to date (also uncommon for a moderately anisotropic framework); Brillouin spectroscopic measurements (*e.g.* Ref.13) are warranted in future to unambiguously confirm this theoretical result.

Given that experimental measurements of single-crystal elastic constants C_{ij} 's can be challenging and often intractable for low-symmetry systems, the application of DFT to probe the elasticity of MOFs is definitely attractive and has become increasingly popular. Certain elasticity measurements, however, such as the Young's modulus (E from single-crystal nanoindentation), bulk modulus and linear compressibility information (*e.g.* K and β from high-pressure crystallography) are nowadays becoming more accessible. We therefore strongly recommend the use of at least some of the aforementioned mechanical properties for basic verifications of any theoretical outcomes. This is an essential step for demonstrating that any theoretical projections are indeed physically meaningful.

Notes and references

^a Department of Engineering Science, University of Oxford, Parks Road, Oxford OX1 3PJ, United Kingdom. *Email: jin-chong.tan@eng.ox.ac.uk

^b Department of Chemistry, NIS and INSTM Reference Centre, University of Turin, via P. Giuria 7, 10125 Torino, Italy. ³Email: bartolomeo.civalleri@unito.it

†Electronic Supplementary Information (ESI) available: DFT computational details. Lattice parameters of optimised geometry. Elastic compliance tensors S_{ij}^* s. See DOI: 10.1039/c000000x/

References

1. K. S. Park, Z. Ni, A. P. Cote, J. Y. Choi, R. D. Huang, F. J. Uribe-Romo, H. K. Chae, M. O'Keeffe and O. M. Yaghi, *Proc Natl Acad Sci USA*, 2006, **103**, 10186-10191.
2. Y. Q. Tian, Y. M. Zhao, Z. X. Chen, G. N. Zhang, L. H. Weng and D. Y. Zhao, *Chem Eur J*, 2007, **13**, 4146-4154.
3. H. Furukawa, K. E. Cordova, M. O'Keeffe and O. M. Yaghi, *Science*, 2013, **341**, 974-986; M. R. Ryder and J. C. Tan, *Mater Sci Tech*, 2014, **30**, 1598-1612.
4. A. Phan, C. J. Doonan, F. J. Uribe-Romo, C. B. Knobler, M. O'Keeffe and O. M. Yaghi, *Accounts Chem Res*, 2010, **43**, 58-67.
5. J. C. Tan and A. K. Cheetham, *Chem Soc Rev*, 2011, **40**, 1059-1080.
6. D. F. Bahr, J. A. Reid, W. M. Mook, C. A. Bauer, R. Stumpf, A. J. Skulan, N. R. Moody, B. A. Simmons, M. M. Shindel and M. D. Allendorf, *Phys Rev B*, 2007, **76**; S. Henke, W. Li and A. K. Cheetham, *Chem Sci*, 2014, **5**, 2392-2397.
7. J. C. Tan, T. D. Bennett and A. K. Cheetham, *Proc Natl Acad Sci USA*, 2010, **107**, 9938-9943.
8. J. C. Tan, C. A. Merrill, J. B. Orton and A. K. Cheetham, *Acta Mater*, 2009, **57**, 3481-3496.
9. B. Van de Voorde, R. Ameloot, I. Stassen, M. Everaert, D. De Vos and J. C. Tan, *J Mater Chem C*, 2013, **1**, 7716-7724.
10. S. Bundschuh, O. Kraft, H. K. Arslan, H. Gliemann, P. G. Weidler and C. Wöll, *Appl Phys Lett*, 2012, **101**, 101910; A. Venkatasubramanian, J.-H. Lee, V. Stavila, A. Robinson, M. D. Allendorf and P. J. Hesketh, *Sens Actuator B-Chem*, 2012, **168**, 256-262.
11. S. Eslava, L. Zhang, S. Esconjauregui, J. Yang, K. Vanstreels, M. R. Baklanov and E. Saiz, *Chem Mater*, 2013, **25**, 27-33; M. D. Allendorf, A. Schwartzberg, V. Stavila and A. A. Talin, *Chem Eur J*, 2011, **17**, 11372-11388; K. Zagorodniy, G. Seifert and H. Hermann, *Appl Phys Lett*, 2010, **97**, 251905.
12. H. Wu, T. Yildirim and W. Zhou, *J Phys Chem Lett*, 2013, **4**, 925-930.
13. J. C. Tan, B. Civalleri, C. C. Lin, L. Valenzano, R. Galvelis, P. F. Chen, T. D. Bennett, C. Mellot-Draznieks, C. M. Zicovich-Wilson and A. K. Cheetham, *Phys Rev Lett*, 2012, **108**, 095502.
14. A. U. Ortiz, A. Boutin, A. H. Fuchs and F.-X. Coudert, *Phys Rev Lett*, 2012, **109**.
15. V. Ishwar Hegde, J.-C. Tan, U. V. Waghmare and A. K. Cheetham, *J Phys Chem Lett*, 2013, **4**, 3377-3381.
16. W. Zhou, H. Wu and T. Yildirim, *Chem Phys Lett*, 2010, **499**, 103-107; A. U. Ortiz, A. Boutin, A. H. Fuchs and F.-X. Coudert, *J Phys Chem Lett*, 2013, **4**, 1861-1865.
17. T. D. Bennett, J. C. Tan, S. A. Moggach, R. Galvelis, C. Mellot-Draznieks, B. A. Reisner, A. Thirumurugan, D. R. Allan and A. K. Cheetham, *Chem Eur J*, 2010, **16**, 10684-10690.
18. T. D. Bennett, P. Simoncic, S. A. Moggach, F. Gozzo, P. Macchi, D. A. Keen, J. C. Tan and A. K. Cheetham, *Chem Commun*, 2011, **47**, 7983-7985.
19. E. C. Spencer, R. J. Angel, N. L. Ross, B. E. Hanson and J. A. Howard, *J Am Chem Soc*, 2009, **131**, 4022-4026.
20. P. Serra-Crespo, A. Dikhtiarenko, E. Stavitski, J. Juan-Alcañiz, F. Kapteijn, F.-X. Coudert and J. Gascon, *CrystEngComm*, 2014; J. M. Ogborn, I. E. Collings, S. A. Moggach, A. L. Thompson and A. L. Goodwin, *Chem Sci*, 2012, **3**, 3011; W. Li, M. R. Probert, M. Kosa, T. D. Bennett, A. Thirumurugan, R. P. Burwood, M. Parinello, J. A. K. Howard and A. K. Cheetham, *J Am Chem Soc*, 2012, **134**, 11940-11943.
21. T. D. Bennett and A. K. Cheetham, *Accounts Chem Res*, 2014, **47**, 1555-1562.
22. T. D. Bennett, A. L. Goodwin, M. T. Dove, D. A. Keen, M. G. Tucker, E. R. Barney, A. K. Soper, E. G. Bithell, J. C. Tan and A. K. Cheetham, *Phys Rev Lett*, 2010, **104**, 115503.
23. T. D. Bennett, P. J. Saines, D. A. Keen, J. C. Tan and A. K. Cheetham, *Chem Eur J*, 2013, **19**, 7049-7055; D. F. Sava, M. A. Rodriguez, K. W. Chapman, P. J. Chupas, J. A. Greathouse, P. S. Crozier and T. M. Nenoff, *J Am Chem Soc*, 2011, **133**, 12398-12401.
24. D. Bazer-Bachi, L. Assié, V. Lecocq, B. Harbuzaru and V. Falk, *Powder Technol*, 2014, **255**, 52-59.
25. E. C. Spencer, R. J. Angel, N. L. Ross, B. E. Hanson and J. A. K. Howard, *J Am Chem Soc*, 2009, **131**, 4022-4026.
26. T. D. Bennett, S. Cao, J. C. Tan, D. A. Keen, E. G. Bithell, P. J. Beldon, T. Friscic and A. K. Cheetham, *J Am Chem Soc*, 2011, **133**, 14546-14549.
27. C. F. Macrae, I. J. Bruno, J. A. Chisholm, P. R. Edgington, P. McCabe, E. Pidcock, L. Rodriguez-Monge, R. Taylor, J. van de Streek and P. A. Wood, *J Appl Crystallogr*, 2008, **41**, 466-470.
28. R. Dovesi, R. Orlando, B. Civalleri, C. Roetti, V. R. Saunders and C. M. Zicovich-Wilson, *Z Kristall*, 2005, **220**, 571-573; R. Dovesi, V. R. Saunders, C. Roetti, R. Orlando, C. M. Zicovich-Wilson, F. Pascale, B. Civalleri, K. Doll, N. M. Harrison, I. J. Bush, P. D'Arco and M. Llunell, *CRYSTAL09 User's Manual*, University of Torino, Torino, (2009).
29. J. P. Perdew, K. Burke and M. Ernzerhof, *Phys Rev Lett*, 1996, **77**, 3865-3868.
30. B. Civalleri, F. Napoli, Y. Noel, C. Roetti and R. Dovesi, *CrystEngComm*, 2006, **8**, 364-371.
31. W. F. Perger, J. Criswell, B. Civalleri and R. Dovesi, *Comput Phys Commun*, 2009, **180**, 1753-1759.
32. J. F. Nye, *Physical Properties of Crystals*, Clarendon Press, Oxford, 1985.
33. A. Marmier, Z. A. D. Lethbridge, R. I. Walton, C. W. Smith, S. C. Parker and K. E. Evans, *Comput Phys Commun*, 2010, **181**, 2102-2115.
34. H. Ledbetter and A. Migliori, *J Appl Phys*, 2006, **100**.
35. W. C. Oliver and G. M. Pharr, *J Mater Res*, 1992, **7**, 1564-1583.
36. J. C. Tan, J. D. Furman and A. K. Cheetham, *J Am Chem Soc*, 2009, **131**, 14252-14254.
37. M. Kosa, J. C. Tan, C. A. Merrill, M. Krack, A. K. Cheetham and M. Parrinello, *ChemPhysChem*, 2010, **11**, 2332-2336.
38. G. N. Greaves, A. L. Greer, R. S. Lakes and T. Rouxel, *Nat Mater*, 2011, **10**, 823-837.
39. Z. A. D. Lethbridge, R. I. Walton, A. S. H. Marmier, C. W. Smith and K. E. Evans, *Acta Mater*, 2010, **58**, 6444-6451.
40. W. Morris, C. J. Stevens, R. E. Taylor, C. Dybowski, O. M. Yaghi and M. A. Garcia-Garibay, *J Phys Chem C*, 2012, **116**, 13307-13312.
41. P. G. Yot, Q. Ma, J. Haines, Q. Yang, A. Ghoufi, T. Devic, C. Serre, V. Dmitriev, G. Férey, C. Zhong and G. Maurin, *Chem Sci*, 2012, **3**, 1100.
42. A. U. Czaja, N. Trukhan and U. Muller, *Chem Soc Rev*, 2009, **38**, 1284-1293.

Graphical & text abstract – Tan *et al.*

We use density functional theory to reveal the detailed elastic properties of two topical ZIF materials comprising the same chemical composition but of differing crystalline structures. ZIF-4 was found to exhibit a negative Poisson's ratio, representing the first 'auxetic-ZIF' to be identified.

